







Open Archive TOULOUSE Archive Ouverte (OATAO)

OATAO is an open access repository that collects the work of some Toulouse researchers and makes it freely available over the web where possible.

This is an author's version published in : <http://oatao.univ-toulouse.fr/13609>

Official URL : <https://doi.org/10.1007/s11004-015-9587-9>

To cite this version :

Guibert, Romain  and Horgue, Pierre  and Debenest, Gérald  and Quintard, Michel  *A comparison of various methods for the numerical evaluation of porous media permeability tensor from pore-scale geometry.* (2016) *Mathematical Geosciences*, vol. 48 (n° 3). pp. 329-347. ISSN 1874-8961

Any correspondence concerning this service should be sent to the repository administrator : tech-oatao@listes-diff.inp-toulouse.fr

A Comparison of Various Methods for the Numerical Evaluation of Porous Media Permeability Tensors from Pore-Scale Geometry

Romain Guibert · Pierre Horgue ·
Gérald Debenest · Michel Quintard

Abstract In this work, several boundary value problems used to numerically evaluate the absolute permeability tensors of porous media using core-scale images are compared and discussed. The various configurations differ by the type of boundary conditions used to compute the flow at the micro-scale. The issue is the ability of the method to capture anisotropy correctly and to avoid possible percolation artifacts. This study is carried on two-dimensional synthetic, isotropic or anisotropic, porous media that are chosen to illustrate the various difficulties mentioned above. A new method is proposed which consists in embedding the porous medium in question in a homoge-nized one. Using an iterative optimization procedure on the surrounding permeability, the method determines the absolute permeability tensor of the original medium. The equivalent permeability tensor that minimizes the effect on the surrounding porous medium is, unlike that of classical methods, de facto symmetrical due to the use of periodic boundary conditions and exhibits significantly lower permeabilities. The way in which non-diagonal terms of the permeability tensor are obtained with the various methods is thoroughly discussed.

Keywords Absolute permeability tensor · Boundary condition configurations · Periodization · Effective medium approach

R. Guibert (✉) · P. Horgue · G. Debenest · M. Quintard
Université de Toulouse, INPT, UPS, IMFT (Institut de Mécanique des Fluides de Toulouse),
Allée Camille Soula, 31400 Toulouse, France
e-mail: romain.guibert@imft.fr

R. Guibert · P. Horgue · G. Debenest · M. Quintard
CNRS, IMFT, 31400 Toulouse, France

1 Introduction

Following the recent progress and increased availability of X-ray computed tomography, together with the development of high-performance computing, the recent literature provides a variety of studies concerning the determination of rock properties from micro-scale imaging (Petrasch et al. 2008; Piller et al. 2009; Khan et al. 2012; Andrä et al. 2013a,b; Blunt et al. 2013; Mostaghimi et al. 2013). In particular, determination of intrinsic permeability is a key feature in petroleum engineering, hydrogeology, geoscience and many other industrial applications. While such computations have indeed accelerated recently and even reached commercial status, the decades-old question of determining effective porous media properties knowing the pore-scale geometry has still not been settled (Adler 1994; Anguy et al. 1994; Spanne et al. 1994; Bogdanov et al. 2003). While there is a consensus on the form of the macro-scale equation to be used for elementary transport processes, such as diffusion or Stokes flows, the computation of the associated effective diffusion or permeability tensors on real images poses several questions which are the subject of this paper. To illustrate the discussion, the case of a one-phase creeping flow is considered here.

The classic macroscopic equation describing the momentum balance for a porous medium can be written using a generalized form of Darcy's law as

$$\mathbf{U} = -\frac{\mathbf{K}}{\mu} \cdot \nabla P, \quad (1)$$

where \mathbf{U} is the average fluid velocity (filtration velocity), μ is the dynamic viscosity of the fluid, ∇P is the macro-scale pressure gradient including the hydrostatic field for sake of simplicity and \mathbf{K} is the permeability tensor, which can be reduced to a scalar for an isotropic medium. Darcy's law is valid for steady-state, single-phase and low Reynolds number. While it has been determined experimentally and proposed in a relatively heuristic way (Darcy 1856), its theoretical basis has already been rigorously demonstrated using various upscaling techniques (Sanchez-Palencia 1982; Whitaker 1986) and does not raise questions, at least for stationary porous media far from singularities or boundaries. The macro-scale permeability tensor is related to the micro-scale geometry through the resolution of a closure problem, which has the structure of a Stokes problem and makes use of periodic boundary conditions for the velocity and the pressure deviation of the linear macro-scale pressure field. If the medium is truly periodic, which may be the case for some manufactured or reconstructed media, the application of the theory is straightforward and requires resolution only over the periodic unit cell. For a given sample of a real porous medium, this is in general not the case since the sample external surface necessarily intersects solid and fluid phases in a non-periodic fashion and, therefore, periodic boundary conditions cannot be applied directly.

Moreover, the validity of the permeability, determined numerically or experimentally, is linked with the question of the representativeness of the considered sample. This is connected with the estimation of a representative elementary volume (REV) which is the minimal volume characterized by the emergence of an equivalent

permeability which will remain constant if calculated on larger volumes. The first condition to be satisfied is to deal with percolating samples and this is not guaranteed for small images of media with low porosity values, even if the medium is permeable at the investigated core scale. If this percolation condition is satisfied, the determination of permeability using a permeameter configuration (Renard et al. 2001), for example, is then possible. Increasing the sample size under such conditions should lead to a robust estimation of the effective permeability of the medium. Intuitively, one assumes that the REV should be much larger than the correlation length associated with the phase indicator. Unfortunately, this is not a sufficient condition since the choice of the boundary conditions on the REV surface may pose problems. For instance, the use of periodic conditions will, in fact, change the statistical properties of the original medium by reproducing the REV structure periodically, thus affecting the semi-variogram of the phase indicator, or even, in some cases, leading to a non-percolating structure. This situation may have a drastic impact on the computed effective permeability as will be discussed later in this paper.

The determination of a representative medium may proceed in different ways: computation of permeability for different samples of different sizes, for subsamples of big enough samples. Whatever the strategy, the requirement is to estimate a permeability from a given image and to do so with minimum biases. The most common solution to numerically determine the components of the permeability tensor on such objects is to solve the fluid flow equations at the pore-scale on the sample using the classical conservation and momentum equations, and then deduce the upscaled properties by averaging the micro-scale fields. For that purpose, the set of bulk equations must be completed with appropriate boundary conditions and this is where different configurations are possible. Discussing this choice of boundary conditions is the main contribution of this paper.

The first approach considers that the sample is surrounded by other identical samples and, consequently, that periodic boundary conditions can be imposed. This approach fits very well with the use of periodic conditions in the theoretical framework discussed above (Sanchez-Palencia 1982; Whitaker 1986). Unfortunately, as previously mentioned, the use of periodicity is likely to change the statistical features of the media studied, at least in principle. This is discussed more specifically below.

Two possible procedures (translation or symmetry) have been devised to make the medium periodic as illustrated in Fig. 1. Periodization by translation is the most commonly used (Whitaker 1986) as it looks a priori attractive a priori: it does not seem to affect the orientation of the geometrical features, at least. However, this procedure may create non-percolating media as illustrated in Fig. 1a, which can indeed be considered as a drastic bias in the permeability determination process. This risk of non-percolation is less probable for a three-dimensional porous medium, but cannot be completely neglected, particularly for porous media with low porosity. The second procedure proposed and discussed in this study, periodization by symmetry (Fig. 1b), allows periodic and percolating samples to be constructed. However, this increases the computational domain and also potentially changes the statistical properties of the medium. In Fig. 1, it is easy to visualize transverse flows being annihilated by

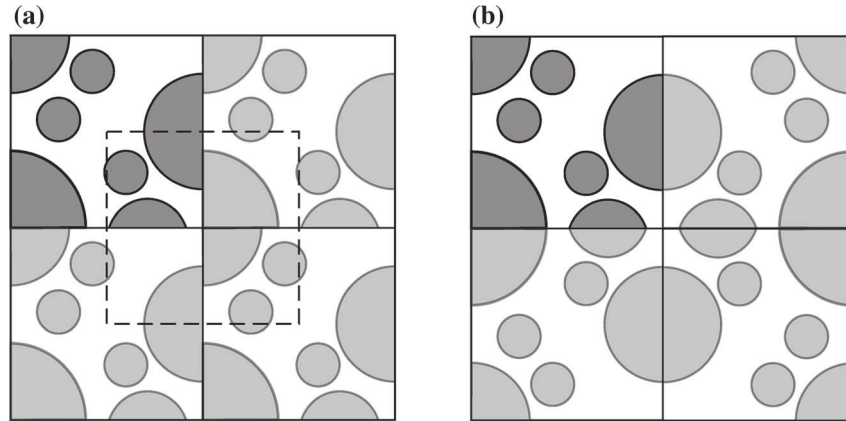


Fig. 1 Sketch of periodization: **a** by translation and **b** by symmetry

the symmetry operation, thus killing most of the anisotropy features of the resulting effective permeability tensor which can also be considered as a serious bias.

In an attempt not to change the medium geometry, a second approach consists in imposing pressure on inlet and outlet sample boundaries (pressure, velocity or flux imposed depending on the method, see Sect. 2). These conditions, denoted pressure-imposed configurations (sometimes called permeameter conditions by reference to the measurement of permeability), are widely used in upscaling studies (Long et al. 1982; Renard and de Marsily 1997; Bailly et al. 2009; Pouya and Fouché 2009) over various types of media and are also widely applied for the treatment of micro-scale images (Mostaghini et al. 2013 for example).

In this work, these different methods, classified as pressure imposed or periodic configurations, are compared. Our aim is (i) to compare the main permeabilities (diagonal terms of the tensors) and (ii) to investigate the potential loss of non-diagonal terms of the permeability tensor. To clearly understand these effects and benchmark all the proposed methods, simple idealized porous media are chosen to enhance the features of particular interest for our discussion. In addition to the more conventional methods, a new approach is proposed for the permeability evaluation, inspired from the effective medium approach (EMA) (Stroud 1975). This method is based on the embedding of the considered pore-scale structure in a controlled homogeneous porous medium treated at the macro-scale. This method has the advantage of enabling the use of periodic conditions without a periodization procedure. Although there are still potential artifacts since this approach more or less tends to modify the medium statistical properties to a greater or lesser extent, it is expected to produce less severe constraints than the other methods.

The paper is constructed as follows: the configurations, the mathematical models and the numerical methods are described in Sect. 2 and in Sect. 3, the results of comparisons between the various methods are presented for isotropic and anisotropic porous media.

2 Materials and Methods

To numerically evaluate the permeability in Eq. (1), it is necessary to solve the fluid flow equations at the micro-scale. The flow is described by Stokes equation and, neglecting gravity (the hydrostatic pressure field can easily be included in a modified pressure definition), the conservation and momentum equations are written as

$$\nabla \cdot \mathbf{u} = \mathbf{0} \quad \text{in } V_f, \quad (2)$$

$$\mu \Delta \mathbf{u} = \nabla p \quad \text{in } V_f, \quad (3)$$

where V_f is the fluid volume. A no-slip condition must be satisfied at the fluid–solid interface A_{fs}

$$\mathbf{u} = \mathbf{0} \quad \text{at } A_{fs}, \quad (4)$$

where $\mathbf{u}(\mathbf{x})$ is the velocity field, $p(\mathbf{x})$ the pressure and μ the dynamic viscosity of the fluid. These equations must be completed with boundary conditions at A_{fe} , representing the entrances and exits of the fluid domain. As explained in Sect. 1, two main approaches with several variants may be proposed, which differ in terms of the assumptions made at the sample boundaries A_{fe} . Furthermore, three calculations are necessary, one for each spatial directions, to determine the complete permeability tensor \mathbf{K} .

These different configurations are presented in the following sub-sections. Note that, to complete the sets of boundary conditions presented, when a Dirichlet condition is imposed on one of the two variables, a homogeneous Neumann condition is imposed on the other. When a periodic condition is prescribed, the periodicity is imposed on both the two variables and a reference pressure must be assigned inside the computational domain.

2.1 Pressure-Imposed Configurations

Here, the three pressure-imposed configurations, which will be used and compared in Sect. 3, are summarized in Fig. 2 and detailed below.

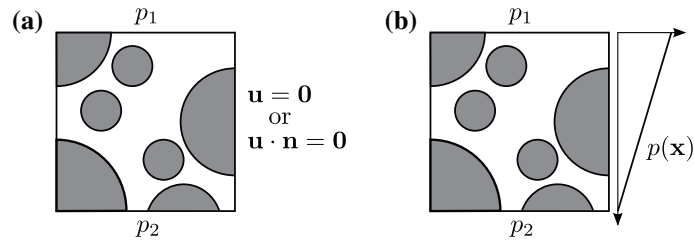


Fig. 2 Illustrations of pressure boundary conditions' configurations: **a** fixed pressure and **b** linear pressure boundary conditions

2.1.1 Fixed Pressure Boundary Conditions with Walls (P_{FW})

This set of boundary conditions (Fig. 2a) is the most common configuration used to characterize the absolute permeability of rocks (Spanne et al. 1994; Mostaghini et al. 2013). A pressure difference is imposed through the domain, fixing two different values for two parallel boundaries (inlet and outlet). On the other boundaries, a no-slip velocity condition is imposed to represent walls. This configuration reproduces the experimental setup of a permeameter (Renard et al. 2001). Since flow is not allowed in the transverse direction, this method is expected to potentially kill anisotropy effects that are not along the computational axes.

2.1.2 Fixed Pressure Boundary Conditions with Symmetries (P_{FS})

This configuration is a simple variant of the previous one (Fig. 2a), where the lateral boundaries are symmetry planes, thus allowing for some slip over the related portion of A_{fe} . Nevertheless, the transverse flow is zero and this method suffers from the same drawback as the previous one in terms of anisotropy effects.

2.1.3 Linear Pressure Boundary Conditions (P_L)

This less common configuration imposes a linear pressure drop on the lateral faces of the sample in conjunction with the imposed pressures at the inlet and outlet (Fig. 2b). This method was first proposed by Bamberger (Bamberger 1977). Although this configuration (Long et al. 1982; Pouya and Fouché 2009) is generally used for the so-called second upscaling procedure where Darcy's law is used as the micro-scale equation, it is also possible to use it at the microscopic scale. This method models the immersion of the REV in a larger volume and allows for transversal flows (contrary to the previous methods). For the second upscaling procedure, it has been observed that this method reproduces some anisotropy effects blocked by the previous methods.

2.2 Periodic Configuration (P)

Another possibility is to solve the closure problem arising from Stokes equation using the original problems proposed by the homogenization or volume averaging theories (Whitaker 1986; Quintard and Whitaker 1989; Sanchez-Palencia 1982). In this case, periodic boundary conditions are imposed on the pressure deviation and the velocity fields. The medium also needs to be periodized and two procedures have been proposed: by translation and by symmetrization (Fig. 1). It has already been noted that the periodization by translation cannot be used if this results in A_{fe} being covered by the solid phase, thus creating a non-percolating medium. Even if this is not exactly the case, it is clear that a drastic decrease of the A_{fe} fluid surface would decrease the computed permeability in an artificial way. Therefore, the symmetrization procedure will be used because A_{fe} with solid parts is the most current situation. The pressure deviation is defined as

$$\nabla p = \overline{\nabla p} + \nabla \tilde{p}, \quad (5)$$

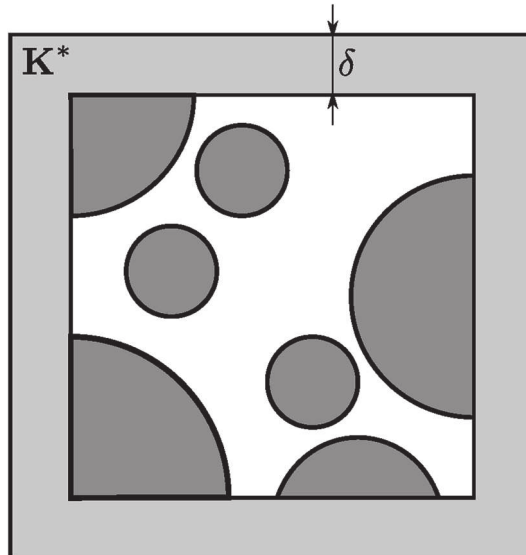
with $\overline{\nabla p}$ an average pressure gradient and $\nabla \tilde{p}$ the computed deviation of the pressure gradient. The average pressure gradient is a volume source term and the deviation needs a pressure reference value (fixed at the outlet for example), or, more physically understandable, but not necessary, a condition of zero average value. This procedure is very close to the original problem proposed by Sanchez-Palencia (1982) to compute the permeability tensor. The closure problem developed in Whitaker (1986) is slightly different, but can be recast into a similar problem by following the indications in Lasseux et al. (1996).

2.3 Effective Medium Approach (*E*)

The main idea of this method, which can be seen as a generalization of the volume averaging approach, is to embed the medium in question in a homogenized porous medium of thickness δ , characterized and controlled by a user-defined permeability tensor \mathbf{K}^* (Fig. 3). By varying \mathbf{K}^* , the objective of the method is to converge to the case where the imposed permeability of the surrounding porous medium is equal to the global permeability of the whole sample. One can then consider that this value is very close to the permeability tensor of the sample. The procedure for optimizing the tensor \mathbf{K}^* , and the sensitivity to the parameter δ , is detailed in Sect. 3.2.

As for the method presented above, periodic boundary conditions are used with a volume source term corresponding to the average pressure gradient. Due to the presence of a homogeneous porous medium around the sample, the percolating condition is no longer necessarily contrary to usual “periodic” approaches and can, therefore,

Fig. 3 Illustration of the effective medium approach, involving the permeability \mathbf{K}^* and the thickness δ of the surrounding porous medium



be used on any sample. This method is expected to provide less bias, in terms of anisotropy, than the other methods.

From a mathematical point of view, the core-scale problem contains both fluid and porous regions with different momentum equations (Stokes or Darcy). A fictitious domain approach (Khadra et al. 2000) is chosen to obtain unique set of equations for the whole domain. It consists in penalizing the momentum equation with a Darcy drag term

$$\mu \left(\Delta \mathbf{u} - \mathbf{K}^{*-1} \cdot \frac{\mathbf{u}}{\Pi} \right) = \nabla p, \quad (6)$$

to obtain the Brinkman equation where only one viscosity μ is considered. The penalization term Π is defined by

$$\Pi = \begin{cases} \Pi \rightarrow +\infty & \text{in the fluid region} \\ 1 & \text{in the porous region.} \end{cases} \quad (7)$$

The idea behind the proposed method is reminiscent of the ideas found in Effective Medium Theories (EMT) (Bruggeman 1935; Landauer 1952; Stroud 1975, 1998), which were developed for diffusive problems. The application to the problem described by Eq. (6) or a somewhat similar problem corresponding to a medium made up of Stokes and Darcy domains requires the macro-scale model to have the structure of Darcy's law. This is indeed the case, as has been demonstrated in Arbogast and Lehr (2006), Popov et al. (2009), Huang et al. (2011), Golfier et al. (2014). Furthermore, while the EMT original development makes use of inclusions embedded in an *infinite* effective medium, the embedding domain here has a finite size. It is merely used to relax the percolation problems discussed above and constraints will have to be verified to avoid dependency of the resulting effective permeability tensor on the choice of the embedding porous domain.

2.4 Determination of Permeability Tensor

For all the configurations, the Darcy velocity is reconstructed from the spatial average of the local velocity field as follows

$$\langle \mathbf{u}(\mathbf{x}) \rangle = \frac{1}{V_t} \int_{V_f} \mathbf{u}(\mathbf{x}) dV, \quad (8)$$

where V_t and V_f stand for the total and fluid volumes, respectively. Then, from two computations of velocity fields ($[u_x^1, u_y^1]$ and $[u_x^2, u_y^2]$), corresponding to imposed pressure gradients in the x - and y -directions (∇p_x^1 and ∇p_y^2), it is possible to reconstruct the full permeability tensor \mathbf{K} using Darcy's law [Eq. (1)] and solving the following linear system

$$\begin{pmatrix} K_{xx} & K_{xy} \\ K_{yx} & K_{yy} \end{pmatrix} \begin{pmatrix} \overline{\nabla p_x^1} & \overline{\nabla p_x^2} \\ \overline{\nabla p_y^1} & \overline{\nabla p_y^2} \end{pmatrix} = \mu \begin{pmatrix} \langle u_x^1 \rangle & \langle u_x^2 \rangle \\ \langle u_y^1 \rangle & \langle u_y^2 \rangle \end{pmatrix}, \quad (9)$$

where ∇p_x^2 and ∇p_y^1 are the transverse pressure gradients not imposed, but computed from simulations in the pressure-imposed configuration (P_{F_w}, P_{F_s} and P_L). Note that, for periodic configurations (P and E), the transverse pressure gradients are equal to zero and then the linear system can be expressed as four independent equations. Although the fluxes across lateral faces are equal to zero in the permeameter case, the averaged velocity field has non-zero transversal components, which implies a non-diagonal permeability tensor. More generally, for all pressure-imposed configurations, the numerically computed permeability tensor is not necessarily symmetrical as observed by previous authors (Manwart et al. 2002; Piller et al. 2009). However, it should be noted that periodic conditions on pressure and velocity fields lead to a symmetrical permeability tensor (Bakhvalov and Panasenko 1989).

In any case, Eq. (1) together with the total mass balance equation allows us to write, in the case of a constant viscosity and permeability tensor

$$\nabla \cdot \mathbf{V} = 0 \Rightarrow \mathbf{K} : \nabla \nabla P = 0. \quad (10)$$

Since $\nabla \nabla P$ is symmetric, this implies that

$$\mathbf{K} : \nabla \nabla P = \frac{1}{2} (\mathbf{K} + \mathbf{K}^T) : \nabla \nabla P = 0, \quad (11)$$

which, in turn, implies that only the symmetrical part of the permeability tensor plays a role [which is consistent with arguments coming from the principles of the thermodynamics of irreversible processes (Marle 1965)]. While several procedures may be proposed to force symmetry from non-symmetric tensors, see for example the work of Durlofsky (2005), the most consistent method is to take the symmetrical part $\frac{1}{2}(\mathbf{K} + \mathbf{K}^T)$.

2.5 Porous Media Studied

Simple two-dimensional synthetic porous media were designed to compare existing methods and test the newly proposed one. The medium domains are square and differ simply by the structure of the solid part, with the idea of emphasizing the different biases identified in the theoretical discussion.

The isotropic media (A1 and A2 in Fig. 4) are formed with 8×8 regular solid bodies where the body width and the space between them are equal to the characteristic length l_c . The two configurations A1 and A2 illustrated in Fig. 4 correspond to the same sample and differ simply by the region considered, in other words the boundary regions. This sample has a width of $16 \times l_c$ and a porosity of 0.75.

The anisotropic medium B1 (Fig. 4) is constructed from the isotropic sample by adding some supplementary solid objects, so that all symmetry axes are broken. The sample exhibits the same correlation length and has a porosity of 0.629. Note that, the permeability of the media A1 and A2 can be considered as a scalar whereas it will be necessary to compute a full permeability tensor for the anisotropic medium B1.

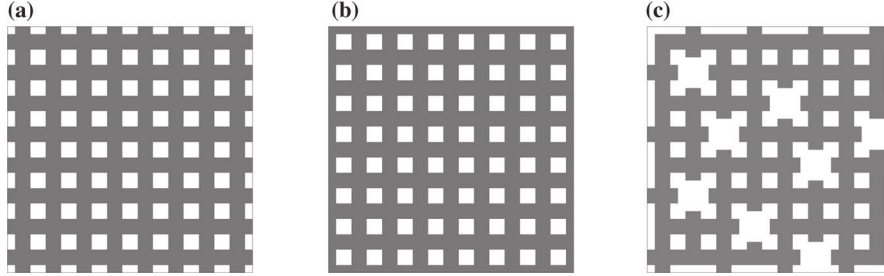


Fig. 4 Synthetic two-dimensional porous media: isotropic media **a** A1, **b** A2, respectively, with fluid/solid and purely fluid boundary conditions and **c** anisotropic medium B1 (non-percolating by translation)

2.6 Numerical Methods

Computations are performed using the open-source finite volume CFD toolbox OpenFOAM[®]. A SIMPLE (semi-implicit method for pressure linked equations) algorithm is generally used to solve Stokes or Brinkman equations. Our solver features some changes compared to the basic version of the `simpleFoam` solver provided: volume source terms for the pressure gradient, tensorial penalization terms and permeability evaluations. Concerning the effective medium approach in the tensorial penalization case (for an anisotropic medium), a PISO (pressure implicit with splitting of operator) solver is necessary to ensure convergence (based on the `pisoFoam` solver provided). Although the desired solution is stationary, the SIMPLE algorithm does not converge in that configuration and we assume that this is due to the discontinuity between the porous and fluid regions. However, for each change in the imposed permeability of the surrounding porous medium, simulations start with the last known fields which allow fast convergence of the transient simulations.

The toolbox controls discretization schemes (second order here) and the relative convergence criteria on the pressure computation (10^{-12} in our case).

3 Results and Discussion

In this section, the results of permeability computations made on the synthetic porous media introduced in Sect. 2.5 are presented and discussed.

3.1 Preliminaries: Mesh Sensitivity

The same algorithm and numerical schemes are used for all configurations and the characteristic length l_c , representing the size of the passages between two obstacles, is similar for all the porous media (A1, A2 and B1). For these reasons, and assuming that the accuracy is mainly related to the number of cells used to discretize the passage width, the mesh sensitivity study is performed on a single configuration P_{Fw} for the regular porous medium A1. The permeability values computed in that case are compared for three refinements (Table 1).

A relative error close to 1 %, compared to the result with the finest grid, is observed on the permeability for the second refinement level mesh with a dimensionless cell

Table 1 Mesh sensitivity for the regular porous medium A1 and the configuration P_{FW}

$\frac{\Delta h}{l_c}$ (-)	Elements	$E_r(K)$ (%)
0.1	19,200	5.00
0.05	76,800	1.35
0.025	307,200	–

size $\frac{\Delta h}{l_c} = 0.05$. This refinement is used in the following to limit the computation time.

3.2 Specific Elements of the Effective Medium Method

The effective medium approach needs to introduce three permeability tensors:

- the imposed user-defined permeability tensor \mathbf{K}_i^* used to solve the Brinkman Eq. 6 in the surrounding porous medium.
- the equivalent permeability tensor \mathbf{K}_{eq} of the whole domain (the sample and the embedded porous medium) computed as explained in Sect. 2.4.
- the measured permeability tensor \mathbf{K}_m^* of the surrounding porous medium computed (Eq. 9) from the average velocity in the surrounding porous medium is defined as:

$$\langle \mathbf{u}(\mathbf{x}) \rangle_p = \frac{1}{V_p} \int_{V_p} \mathbf{u}(\mathbf{x}) \, dV, \quad (12)$$

where V_p is the volume of the surrounding porous medium (Fig. 3).

The difference between the imposed (\mathbf{K}_i^*) and the effectively measured (\mathbf{K}_m^*) permeability of the surrounding porous medium is due to the use of the Brinkman model which introduces border effects between the sample and the porous medium. The objective of the proposed method is, for a fixed thickness δ of the surrounding porous medium, to find the tensor \mathbf{K}_m^* that minimizes the difference with the equivalent permeability tensor \mathbf{K}_{eq} for each component. To simplify notations, the optimization procedure is detailed below in the case of an isotropic porous medium (A1 or A2) where the permeability sought is a scalar. The differences with respect to the tensor optimization are then detailed.

In practice, for an isotropic case with a scalar permeability, the optimization consists in minimizing the difference between K_m^* and K_{eq} using a minimum of two initial guesses. Figure 5 plots the different dimensionless permeabilities (\bar{K}_i^* , \bar{K}_m^* and \bar{K}_{eq}) made dimensionless using l_c^2 , as a function of the measured permeability \bar{K}_m^* . Two interpolations (\bar{K}_i^* and \bar{K}_{eq}) are constructed from the first two simulations. The intersection between \bar{K}_{eq} and \bar{K}_m^* gives the permeability sought, while the new permeability to be imposed can be read on the \bar{K}_i^* interpolation (Fig. 5). The interpolations can be refined by successive simulations, and in the cases presented, a series of four simulations was necessary and sufficient to approximate the permeability and brought the relative difference between \bar{K}_{eq} and \bar{K}_m^* to below 1 %. In the case presented, the first imposed guesses were $\bar{K}_i^* = 0.045$ and 0.065 which gave a new

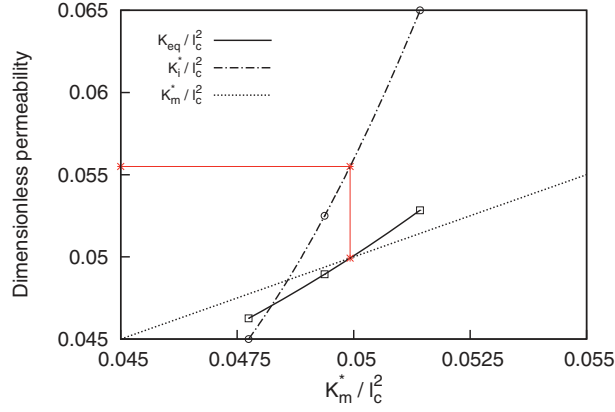
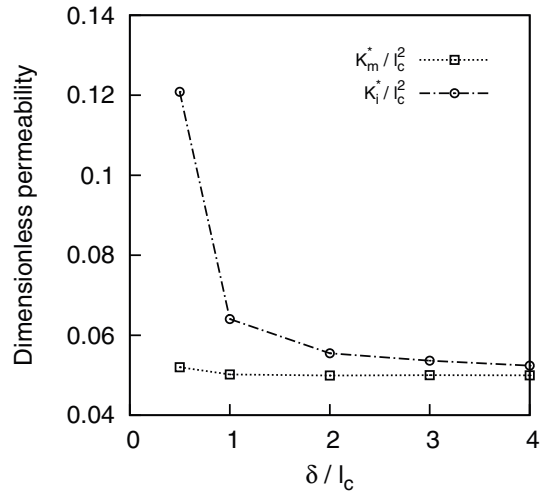


Fig. 5 Illustration of the optimization procedure for configuration *E*, corresponding to the diagonal term of the permeability tensor for the regular medium illustrated in Fig. 4a

Fig. 6 Imposed and measured dimensionless permeabilities function of dimensional porous zone thickness



imposed value $\overline{K}_i^* = 0.0525$. Then, after refining the interpolation with the new simulation, the value to be imposed was $\overline{K}_i^* = 0.578$ which gave the sample permeability $\overline{K}_{eq} = \overline{K}_m^* = 0.0522$. Appropriate initial guesses can be determined from other configurations.

The procedure illustrated in Fig. 5 corresponds to the case of the isotropic medium (Fig. 4a) for which a scalar form of the permeability is expected, but the procedure for the tensorial case is similar. For one direction, corresponding to one column of the permeability tensor, the values are simultaneously optimized and also require four simulations to converge on the diagonal terms. The off-diagonal terms of the tensor, of lower magnitude, can be refined by additional simulations (two in our case). Figure 6 reports the dependence of the imposed and measured permeabilities as a function of the surrounding porous medium thickness δ .

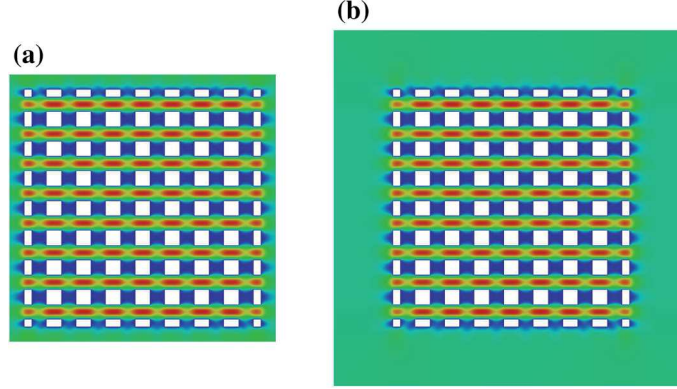


Fig. 7 Two different velocity fields obtained with configuration E for the isotropic medium A1 with **a** $\delta/l_c = 1$ and **b** $\delta/l_c = 4$

When the thickness of the surrounding porous medium increases, the difference between \bar{K}_m^* and \bar{K}_i^* tends to zero, due to the relative reduction of the Brinkman boundary effects (same interface, but higher volume). This effect is emphasized in Fig. 7 which represents the velocity fields obtained using configuration E on medium A1 for different values of δ/l_c . For the larger value of δ/l_c , the velocity heterogeneities are restricted to a relatively small part of the surrounding homogeneous porous medium.

Considering a very large porous medium, it is probably possible to directly optimize the equivalent permeability \bar{K}_{eq} on the imposed value \bar{K}_i^* (because $\bar{K}_i^* = \bar{K}_m^*$ in that case). However, the use of \bar{K}_m^* for the optimization procedure is justified because it strongly limits the thickness δ and, therefore, the computation time. This preliminary case shows that it is reasonable to take a minimal thickness of twice the correlation length l_c related to the sample considered and, therefore, the following numerical simulations are performed with $\delta = 2 \times l_c$.

3.3 Isotropic Medium

The velocity magnitudes for three configurations (P , P_L and E) for the porous medium A1 are presented in Fig. 8. The periodic configuration P is the reference solution. For the configurations P_L and E , some border effects appear, illustrated in Fig. 8b, c, which affect the permeability values.

The scalar permeabilities obtained for the two similar porous media A1 and A2 with the different configurations are reported in Fig. 9. The values are normalized with the solution obtained in the periodic configuration P , which is the exact theoretical solution for such a periodic medium.

For the porous medium A1, where the solid part intersects the sample boundaries (Fig. 4), all the classic methods give very close values. The configuration with a linear pressure drop P_L slightly overestimates the permeability. Considering the porous medium A2 with purely fluid boundary conditions (Fig. 4), border effects are really marked in configuration P_{Fw} (also illustrated in Fig. 10b). The other classic configura-

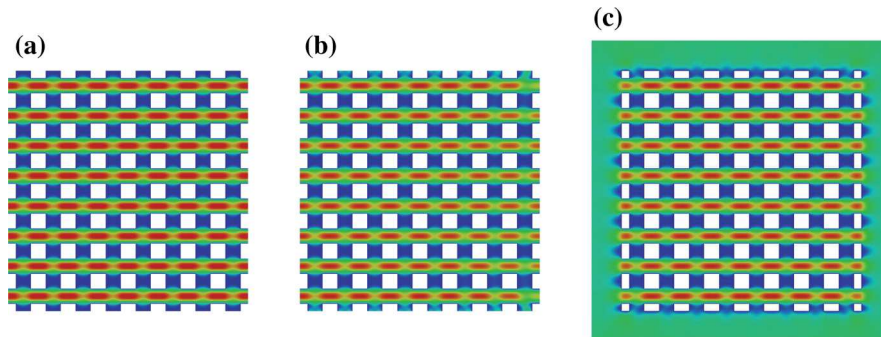
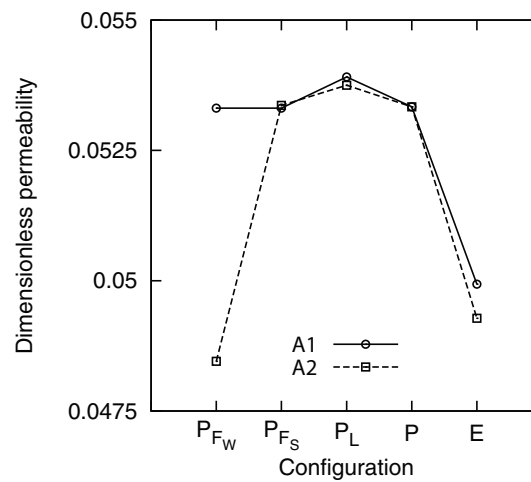


Fig. 8 Velocity field magnitudes for the isotropic medium A1 and different configurations **a** P , **b** P_L and **c** E (the flow is horizontal from *left to right*)

Fig. 9 Comparisons of permeability values obtained with the different configurations



tions keep the same general behavior and give results that are still close to the reference configuration P . We can, therefore, assume that the larger the fluid domain along the sample boundaries, the larger the difference of permeability induced by the no-slip condition (obviously, this would also be the case for the experimental permeameter).

For the effective medium approach, some non-negligible border effects appear due to the mathematical modeling (Figs. 8c, 10c). The relative difference in terms of permeability is around 6 % for the porous medium A1 and around 7 % for the porous medium A2, which points out that the method does not seem to be sensitive to the boundary conditions (fluid/solid or purely fluid). The difference with respect to the periodic configuration is probably mainly related to the size of the sample considered: increasing the fluid volume by studying a larger sample may reduce the influence of border effects.

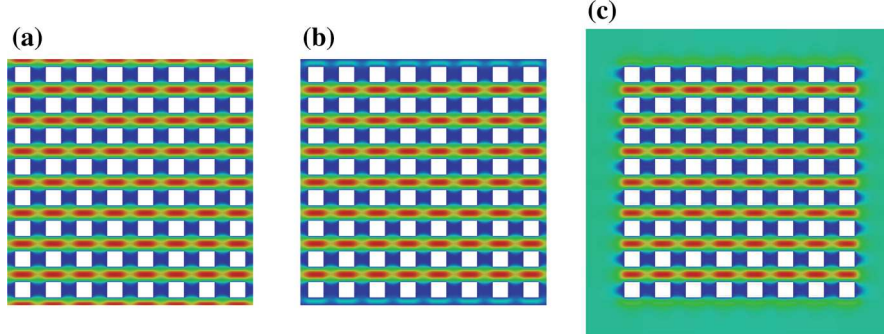


Fig. 10 Velocity field magnitudes for the isotropic porous medium A2 and different configurations **a** P , **b** P_{FW} and **c** E (Fig. 8)

3.4 Anisotropic Medium

The anisotropic porous medium B1, illustrated in Fig. 4, is non-percolating by translation in both spatial directions (which means that, for one spatial direction, the entrance and exit areas are not aligned). As previously discussed in Sect. 1, the direct use of periodic boundary conditions is not possible. So, the sample is made periodic by symmetry (Fig. 1b) to have a percolating medium and use periodic boundary conditions. This configuration is a variant of the periodic configuration P and is noted P_s . Velocity fields obtained with this configuration for the two flow directions are presented in Fig. 11a, b. The figures clearly emphasize the existence of some preferential flow paths.

Regarding this periodic configuration P_s , the permeability can be computed considering two different domains, the initial sample or the full simulation (see Fig. 1b). To compare the different methods, the computed permeability tensor is factorized as follows (in two dimensions)

$$\mathbf{K} = \begin{pmatrix} K_{xx} & K_{xy} \\ K_{yx} & K_{yy} \end{pmatrix} = \max_{i,j} (K_{ij}) \cdot \bar{\mathbf{K}} = l_c^2 \bar{k} \cdot \bar{\mathbf{K}}, \quad (13)$$

where \bar{k} is the dimensionless magnitude and $\bar{\mathbf{K}}$ is the dimensionless tensor. Moreover, for a non-periodic random sample, existing methods systematically produce non-symmetrical permeability tensors for which the asymmetry coefficient d can be defined as follows

$$d = \frac{|\overline{K_{ij}} - \overline{K_{ji}}|}{|\overline{K_{ij}} + \overline{K_{ji}}|} \quad \text{with } i \neq j. \quad (14)$$

The two permeability tensors obtained from the periodic configuration P_s (full domain and sample), as for all the other configurations, are reported in Table 2. The permeability tensors are determined following Eq. 9 and neglecting transverse pressure gradients. The computation of symmetrical off-diagonal terms is determined as

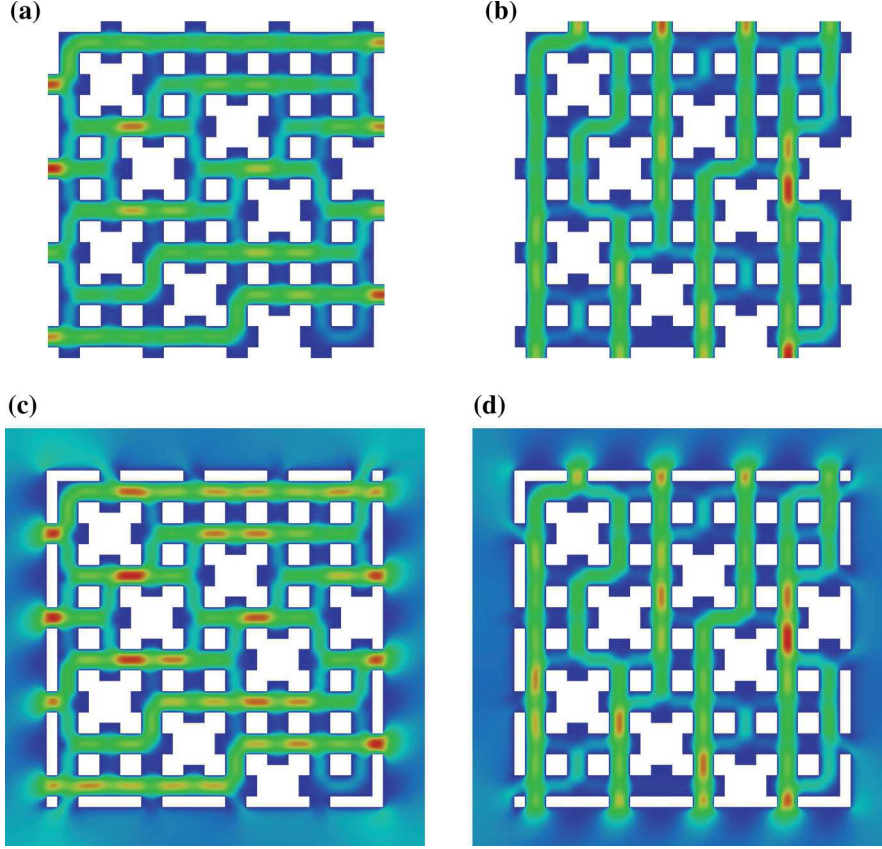


Fig. 11 Illustrations of velocity field magnitudes for **a, b** quarter of configuration P_s and **c, d** full configuration E (the flow is horizontal for **a, c** and vertical for **b, d**)

$$\bar{K}_{\text{sym}} = \frac{1}{2} (\bar{K}_{xy} + \bar{K}_{yx}). \quad (15)$$

As, by construction, the domain symmetrization removes the transverse flow, the permeability tensor in the configuration P_s (full domain) has zero off-diagonal terms. However, averaging performed on the original sample is one possible way to compute a full permeability tensor with non-zero off-diagonal terms. Results in Table 2 denoted P_s (sample) show that, in this case, there is a significant difference between the off-diagonal tensor components. For this clearly anisotropic case, the permeability tensors obtained for P_{F_w} and P_{F_s} are very close to the periodic configuration P_s (sample). Compared with other configurations studied, the linear imposed pressure configuration P_L gives a permeability tensor with higher magnitude and lower off-diagonal terms. Note that, the sign of non-diagonal terms for configuration P_L is different from that in the other configurations. The asymmetry of this method ($d = 0.092$) is of the same order as with the other configurations P_{F_w} , P_{F_s} and P_s . Note that, higher values of asymmetry can be found in the literature (Galindo-Torres et al. 2012). Then, the

Table 2 Permeability tensor components for all configurations studied (neglecting transverse pressure gradients for B , P_s and E)

Configuration	\bar{k}	\bar{K}_{xx}	\bar{K}_{xy}	\bar{K}_{yx}	\bar{K}_{yy}	\bar{K}_{sym}	d
P_{F_W}/P_{F_S}	3.037×10^{-2}	0.992	0.074	0.090	1.000	0.082	0.098
P_L	3.202×10^{-2}	0.974	-0.029	-0.042	1.000	-0.035	0.092
P_s (full domain)	3.038×10^{-2}	0.992	0.0	0.0	1.000	0.0	-
P_s (sample)	3.038×10^{-2}	0.992	0.074	0.090	1.000	0.082	0.098
E	2.443×10^{-2}	0.997	0.082	0.084	1.000	0.083	0.012

Table 3 Permeability tensor components for configurations P_{F_W} , P_{F_S} and P_L using non-zero transverse pressure gradients

Configuration	\bar{k}	\bar{K}_{xx}	\bar{K}_{xy}	\bar{K}_{yx}	\bar{K}_{yy}	\bar{K}_{sym}	d
P_{F_W}/P_{F_S}	3.093×10^{-2}	0.994	-0.099	-0.106	1.000	-0.103	0.034
P_L	3.222×10^{-2}	0.973	-0.089	-0.104	1.000	-0.097	0.078

effective medium approach is tested and Fig. 11c, d shows velocity magnitudes for this configuration. The comparison with the periodic configuration highlights some differences, mainly on the borders of the core-scale sample considered.

As explained in Sect. 3.2, the optimization of one column of the tensor is performed simultaneously and independently for each term of the tensor. However, it is recommended that the difference between the two initial guesses should be less than one order of magnitude to ensure convergence of the optimization. For this, it is possible to use the solution provided by one of the fixed pressure configurations. The permeability tensor obtained by the effective medium approach, reported in Table 2, has a lower magnitude \bar{k} . Note that, the symmetry of the tensor ($d = 0.012$) is not explicitly enforced (optimization of the off-diagonal terms is decoupled and the \mathbf{K}_i^* tensor is non-symmetrical), but is a result of the optimization process. Also, increase in the number of optimization steps progressively decreases the value of d .

The mathematical computation of symmetrical off-diagonal terms \bar{K}_{sym} gives very close results among the various usual methods except for the linear pressure boundary configuration P_L (Table 2). Moreover, the value of \bar{K}_{sym} is close to the almost symmetrical off-diagonal terms of the effective medium approach. In Table 3, permeability tensors are computed taking the non-zero transverse pressure gradients into account (Sect. 2.4). In this form, the three configurations have slightly larger prefactors \bar{k} than in the previous case (Table 2) and lower asymmetry. Note that, configuration P_L has negative off-diagonal terms whereas these terms change sign for permeameter configurations. However, the diagonal part of the reconstructed permeability tensors is all relatively close. The largest differences between configurations are observed on non-diagonal terms. At best, testing several configurations enables a range of values to be determined for off-diagonal terms.

4 Conclusions

A comparison of different configurations, characterized by periodicity or various other pressure boundary conditions, for the numerical evaluation of the permeability tensor has been proposed for isotropic and anisotropic porous media. Two methods have been introduced to apply periodic boundary conditions to a non-periodic, non-percolating sample, which may be the case for a real rock sample. The first method consists in symmetrizing the sample to obtain conformal boundaries suitable for applying periodic boundary conditions. Another method, called the effective medium approach by analogy, has been proposed to complete the set of available methods. This effective medium approach consists in bordering the sample with a homogeneous porous layer of a given thickness and then optimizing a permeability tensor so that the presence of the real sample has no effect on the global permeability. The magnitude of the permeability tensors obtained with this new method is slightly lower in both the isotropic and anisotropic cases.

Concerning the off-diagonal terms, this method allows periodic boundary conditions to be applied and, thus produces de facto a symmetrical permeability tensor without mathematical reconstruction. This is confirmed by the low asymmetry factor, d , obtained in that case compared to the usual configurations (P_{Fw} , P_{Fs} , P_S).

Following the results of the study, the classical method P_{Fw} seems the most suitable method for computing permeability since it produces correct results for both diagonal and off-diagonal terms without requiring excessive computational resources (easy to implement, no specific mesh treatment, etc.). However, these results would require further study on real samples to confirm the observations made.

Acknowledgments This work was supported by the French Research Agency (ANR) through the MOBOPOR project (ANR-10-BLAN-0908).

References

- Adler PM (1994) Porous media: geometry and transport. Butterworth-Heinemann, Stoneham
- Andrä H, Combaret N, Dvorkin J, Glatt E, Han J, Kabel M, Keehm Y, Krzikalla F, Lee M, Madonna C, Marsh M, Mukerji T, Saenger EH, Sain R, Saxena N, Ricker S, Wiegmann A, Zhan X (2013a) Digital rock physics benchmarks—part I: imaging and segmentation. *Comput Geosci* 50:25–32
- Andrä H, Combaret N, Dvorkin J, Glatt E, Han J, Kabel M, Keehm Y, Krzikalla F, Lee M, Madonna C, Marsh M, Mukerji T, Saenger EH, Sain R, Saxena N, Ricker S, Wiegmann A, Zhan X (2013b) Digital rock physics benchmarks—part II: computing effective properties. *Comput Geosci* 50:33–43
- Anguy Y, Bernard D, Ehrlich R (1994) The local change of scale method for modelling flow in natural porous media (I): numerical tools. *Adv Water Resour* 17:337–351
- Arbogast T, Lehr HL (2006) Homogenization of a Darcy–Stokes system modeling vuggy porous media. *Comput Geosci* 10(3):291–302
- Bailly D, Ababou R, Quintard M (2009) Geometric characterization, hydraulic behavior and upscaling of 3D fissured geologic media. *Math Comput Simul* 79(12):3385–3396
- Bakhvalov N, Panasenko G (1989) Homogenisation: averaging processes in periodic media. Springer, Berlin
- Bamberger, A. (1977). Approximation des coefficients d'opérateurs elliptiques stables pour la G-convergence. Technical report
- Blunt MJ, Bijeljic B, Dong H, Gharbi O, Iglauer S, Mostaghimi P, Paluszny A, Pentland C (2013) Pore-scale imaging and modelling. *Adv Water Resour* 51:197–216
- Bogdanov II, Mourzenko VV, Thovert J-F (2003) Effective permeability of fractured porous media in steady state flow. *Water Resour Res* 39:1023–1038

- Bruggeman VDAG (1935) Berechnung verschiedener physikalischer konstanten von heterogenen substanzen. i. dielektrizitätskonstanten und leitfähigkeiten der mischkörper aus isotropen substanzen. *Annalen der Physik* 416:636–664
- Darcy H (1856) *Les Fontaines Publiques de la Ville de Dijon*. Victor Dalmont, Paris
- Durllofsky LJ (2005) Upscaling and gridding of fine scale geological models for flow simulation. In: 8th International forum on reservoir simulation Iles Borromees, Stresa, Italy
- Galindo-Torres SA, Scheuermann A, Li L (2012) Numerical study on the permeability in a tensorial form for laminar flow in anisotropic porous media. *Phys Rev E* 86:046306
- Golfier F, Lasseux D, Quintard M (2014) Investigation of the effective permeability of vuggy or fractured porous media from a Darcy Brinkman approach. *Comput Geosci*. doi:10.1007/s10596-014-9448-5
- Huang Z, Yao J, Li Y, Wang C, Lv X (2011) Numerical calculation of equivalent permeability tensor for fractured vuggy porous media based on homogenization theory. *Commun Comput Phys* 9:180–204
- Khadra K, Angot P, Parneix S, Caltagirone J-P (2000) Fictitious domain approach for numerical modelling of Navier–Stokes equations. *Int J Numer Methods Fluids* 34:651–684
- Khan F, Enzmann F, Kersten M, Wiegmann A, Steiner K (2012) 3D simulation of the permeability tensor in a soil aggregate on the basis of nanotomographic imaging and LBE solver. *J Soils Sediments* 12:86–96
- Landauer R (1952) The electrical resistance of binary metallic mixtures. *J Appl Phys* 23:779–784
- Lasseux D, Quintard M, Whitaker S (1996) Determination of permeability tensors for two-phase flow in homogeneous porous media: theory. *Transp Porous Media* 24(2):107–137
- Long JCS, Remer JS, Wilson CR, Whitherspoon PA (1982) Porous media equivalents for networks of discontinuous fractures. *Water Resour Res* 18:645–658
- Manwart C, Aaltosalmi U, Koponen A, Hilfer R, Timonen J (2002) Lattice-Boltzmann and finite-difference simulations for the permeability for three-dimensional porous media. *Phys Rev E* 66:016702
- Marle C (1965) Application de la méthode de la thermodynamique des processus irréversible à l'écoulement d'un fluide à travers un milieu poreux. *Bull RILEM* 29:1066–1071
- Mostaghini P, Blunt MJ, Bijeljic B (2013) Computations of absolute permeability on micro-CT images. *Math Geosci* 45:103–125
- Petrasch J, Meier F, Friess H, Steinfeld A (2008) Tomography based determination of permeability, Dupuit–Forchheimer coefficient, and interfacial heat transfer coefficient in reticulate porous ceramics. *Heat Fluid Flow* 29:315–326
- Piller M, Schena G, Nolich M, Favretto S, Radaelli F, Rossi E (2009) Analysis of hydraulic permeability in porous media: from high resolution x-ray tomography to direct numerical simulation. *Transp Porous Media* 80:57–78
- Popov P, Efendiev Y, Qin G (2009) Multiscale modeling and simulations of flows in naturally fractured karst reservoirs. *Commun Comput Phys* 6(1):162–184
- Pouya A, Fouché O (2009) Permeability of 3D discontinuity networks: new tensors form boundary-conditioned homogenisation. *Adv Water Resour* 32:303–314
- Quintard M, Whitaker S (1989) écoulement monophasique en milieux poreux : effets des hétérogénéités. *Journal de Mécanique Théorique et Appliquée* 6:691–726
- Renard P, de Marsily G (1997) Calculating equivalent permeability: a review. *Adv Water Resour* 20:253–278
- Renard P, Genty A, Stauffer F (2001) Laboratory determination of the full permeability tensor. *J Geophys Res* 106:443–452
- Sanchez-Palencia E (1982) On the asymptotics of the fluid flow past an array of fixed obstacles. *Int J Eng Sci* 20(12):1291–1301
- Spanne P, Thovert J-F, Jacquín C-J, Lindquist WB, Jones KW, Adler PM (1994) Synchrotron computed microtomography of porous media: topology and transports. *Phys Rev Lett* 73:2001
- Stroud D (1975) Generalized effective-medium approach to the conductivity of an inhomogeneous material. *Phys Rev B* 12:3368–3373
- Stroud D (1998) The effective medium approximations: some recent developments. *Superlattices Microstruct* 23(3):567–573
- Whitaker S (1986) Flow in porous media I: a theoretical deviation of Darcy's law. *Transp Porous Media* 1:3–25